Available online at www.sciencedirect.com
ScienceDirect
International Journal of Thermal Sciences 46 (2007) 479–490
International Journal of Thermal Sciences
www.elsevier.com/locate/ijts

A multiscale Malkmus model for treatment of inhomogeneous gas paths

Sudarshan P. Bharadwaj [a], Michael F. Modest [b,*]

[a] *Impact Technologies, LLC, State College, PA 16801, USA*
[b] *Pennsylvania State University, USA*

Received 30 January 2006; received in revised form 22 June 2006; accepted 26 June 2006

Available online 18 September 2006

Abstract

The Malkmus narrow-band model, while good for homogeneous gas paths, cannot be directly applied to paths with inhomogeneities in temperature, mole fraction and total pressure. The most popular and successful approaches today for dealing with inhomogeneous paths are the Curtis–Godson approximation and the correlated-*k* model. However, these approaches are not accurate for paths with severe inhomogeneities. The current work discusses the development of a multi-scale Malkmus model to overcome these limitations. The model is validated with theoretical data for CO_2 and H_2O obtained from the CDSD and HITEMP databases, respectively.

Keywords: Radiation; Gas; Transmissivity; Nonhomogeneous media

1. Introduction

Narrow-band models were developed to allow radiative heat transfer calculations for gas spectra based on experimental measurements. More recently, after the emergence of high-resolution databases, they remained popular to reduce the computational effort as compared to line-by-line calculations. A number of models have been proposed to model the spacing and strengths of individual lines within a narrow band. The most important ones are the Elsasser model [1–4], which assumes equally-spaced Lorentz lines of equal intensity, and the statistical models [5–10], which postulate a random arrangement of lines and either equal intensity (uniform statistical model [6,7]), random intensities chosen from an exponentially decaying distribution (Goody statistical model [7]), or an inverse probability distribution of line strengths with exponential tails (the Malkmus model [11]).

Several methods exist today to deal with inhomogeneous gas paths. The most popular of these are the Curtis–Godson (CG) approximation [2,12] and the correlated-*k* approach [13]. The CG approximation yields expressions for the narrow-band transmissivity in terms of path-averaged narrow-band parameters, which may be obtained from any of the above narrow-band models. Mixture parameters may be calculated for mixtures of absorbing gases, which may then be averaged over the path to yield transmissivities. Narrow-band model parameters may also be used to derive *k*-distributions, which may be used to obtain the transmissivities of inhomogeneous paths. However, these methods are inaccurate for paths with severe inhomogeneities.

In the current work, a new multi-scale Malkmus model has been developed (as an extension of the single-scale Malkmus model), to handle inhomogeneous gas paths. The parameters for this model may be derived either from experiment or from line-by-line databases.

The remainder of this section provides a brief discussion of the current state-of-the-art methods to deal with inhomogeneous gas paths. The following two sections discuss the development and validation, respectively, of the multi-scale Malkmus (MSM) model, while the last section presents some sample comparisons between the MSM model and the CG and *c*–*k* approaches.

1.1. The Malkmus model

This section briefly reviews the Malkmus narrow-band model as it pertains to the MSM model development. A more detailed discussion may be found in [11]. The Malkmus model

* Corresponding author.
E-mail address: mfmodest@psu.edu (M.F. Modest).

1290-0729/$ – see front matter
doi:10.1016/j.ijthermalsci.2006.06.015

postulates a probability distribution function of line intensities as

$$p(S) = \frac{1}{\ln R} S^{-1}\left[\exp\left(-\frac{S}{S_M}\right) - \exp\left(-\frac{RS}{S_M}\right)\right] \tag{1}$$

where S is the line intensity, and R is the ratio of the maximum intensity to the minimum, i.e., $R = S_M/S_m$. The mean value of S is given by

$$\mathbf{S} = \int_0^\infty Sp(S)\,\mathrm{d}S = \left[\frac{R-1}{R\ln R}\right] S_M \tag{2}$$

The narrow-band transmissivity is obtained as follows. The equivalent width of a single spectral line is defined as

$$W(S,X) = \int \left[1 - \exp\bigl(-\kappa(\eta)X\bigr)\right]\mathrm{d}\eta \tag{3}$$

where η is wavenumber, $\kappa(\eta)$ is the spectral absorption coefficient of a single line, X is the pressure path length (given by the product of the gas partial pressure and the length of the gas column), and $S = \int \kappa(\eta)\,\mathrm{d}\eta$. The mean value of $W(S,X)$ for a group of lines whose intensities are given by a probability distribution function $p(S)$ is

$$\overline{W} = \int W(S,X)p(S)\,\mathrm{d}S \tag{4}$$

Assuming Lorentz broadening,

$$\kappa(\eta) = \frac{Sb/\pi}{(\eta-\eta_0)^2 + b^2} \tag{5}$$

where η_0 is the wavenumber of the line center and b is the half-width at half-height. The equivalent width of a Lorentz-broadened line is

$$W = SX\exp\left(-\frac{SX}{2\pi b}\right)\left[I_0\left(\frac{SX}{2\pi b}\right) + I_1\left(\frac{SX}{2\pi b}\right)\right] \tag{6}$$

where I_0 and I_1 are modified Bessel functions of order 0 and 1, respectively. For the probability distribution function given by Eq. (1), the mean equivalent line width is found to be

$$\frac{\overline{W}}{d_L} = \frac{2\pi b}{d_L \ln R}\left[\left(1 + \frac{R\ln R\mathbf{S}X}{(R-1)\pi b}\right)^{1/2} - \left(1 + \frac{\ln R\mathbf{S}X}{(R-1)\pi b}\right)^{1/2}\right] \tag{7}$$

where $\mathbf{S}$ is the mean line intensity and d_L is the average line spacing. Two parameters S_E and d may now be defined, so as to provide the correct equivalent line width in the limits of both small and large X. Thus,

$$S_E = \mathbf{S}\frac{\ln R}{\pi}\frac{R^{1/2}+1}{R^{1/2}-1} \tag{8}$$

and

$$d = d_L\frac{\ln R}{\pi}\frac{R^{1/2}+1}{R^{1/2}-1} \tag{9}$$

where S_E and d are the "effective" line intensity and spacing, respectively. In terms of S_E and d, in the limit of $R \to \infty$,

$$\frac{\overline{W}}{d} = \frac{b/d}{\pi}\left[\left(1 + \frac{S_E X}{b}\right)^{1/2} - 1\right] \tag{10}$$

The narrow-band transmissivity is then,

$$\overline{\tau} = \exp\left(-\frac{\overline{W}}{d}\right) = \exp\left[-\frac{b/d}{\pi}\left\{\left(1 + \frac{S_E X}{b}\right)^{1/2} - 1\right\}\right] \tag{11}$$

or,

$$\begin{aligned}\overline{\tau} &= \exp\left[-\frac{\pi b_L}{2d}\left\{\left(1 + \frac{4\overline{S}X}{\pi b_L}\right)^{1/2} - 1\right\}\right] \\ &= \exp\left[\frac{\beta}{2}\left\{(1+4t/\beta)^{1/2} - 1\right\}\right]\end{aligned} \tag{12}$$

where $\overline{S} = S_E/2\pi$ is the line intensity parameter, $b_L = 2b/\pi^2$ is the broadening parameter, $t = (\overline{S}/d)X$ is the mean optical thickness, and $\beta = \pi b_L/d$ is the line overlap parameter. For binary mixtures consisting of an absorbing gas and a nonabsorbing gas (usually air or nitrogen), the latter parameter depends on the gas mole fraction x as $b_L = b_{Ls}x + b_{La}(1-x)$, where b_{Ls} is the self-broadening half-width and b_{La} is the air-broadening half-width. This model has been found to work well for homogeneous paths.

1.1.1. k-distributions

The k-distribution method is an alternative to the narrow-band models to perform radiative heat transfer calculations. The method is based on reordering the spectral absorption coefficient over a spectral interval (which may be a narrow-band, wide-band, or the entire spectrum), based on its frequency of occurrence within the interval. This frequency distribution function may then be integrated to obtain the cumulative k-distribution function $g(k)$, which is representative of the fraction of the spectral interval, over which the absorption coefficient has a value less than k. While k-distributions are often derived from line-by-line databases, the above Malkmus parameters may also be used to obtain k-distributions. The cumulative density distribution of absorption coefficient strengths is given by [1]

$$\begin{aligned}g(k) = {}& \frac{1}{2}\mathrm{erfc}\left[\frac{\beta^{1/2}}{2}\left(\left(\frac{\overline{\kappa}}{k}\right)^{1/2} - \left(\frac{k}{\overline{\kappa}}\right)^{1/2}\right)\right] \\ &+ \frac{1}{2}e^{\beta}\mathrm{erfc}\left[\frac{\beta^{1/2}}{2}\left(\left(\frac{\overline{\kappa}}{k}\right)^{1/2} + \left(\frac{k}{\overline{\kappa}}\right)^{1/2}\right)\right]\end{aligned} \tag{13}$$

where $\overline{\kappa} = \overline{S}/d$ is a mean absorption coefficient. This $g(k)$ function may be numerically inverted to obtain the $k(g)$ function. The narrow-band transmissivity may then be calculated for homogeneous paths as

$$\overline{\tau}(X) = \int_0^1 \exp\bigl(-k(g)X\bigr)\,\mathrm{d}g \tag{14}$$

1.2. Inhomogeneous gas paths

This section briefly discusses two of the current state-of-the-art approaches for dealing with inhomogeneous paths, viz., the Curtis–Godson approximation [2,12] and the correlated-k approach [13].

1.2.1. The Curtis–Godson approximation

This method, when coupled with the Malkmus model, yields an expression for the narrow-band transmissivity in terms of path-averaged parameters, $\tilde{t}$ and $\tilde{\beta}$, as

$$\overline{\tau} = \exp\left\{-\frac{\tilde{\beta}}{2}\left[(1+4\tilde{t}/\tilde{\beta})^{1/2}-1\right]\right\} \tag{15}$$

where

$$\tilde{t} = \int_0^X \frac{\overline{S}}{d}\,\mathrm{d}X \tag{16}$$

and

$$\tilde{\beta} = \frac{1}{\tilde{t}}\int_0^X \frac{\overline{S}}{d}\beta\,\mathrm{d}X \tag{17}$$

For gas mixtures, the corresponding Malkmus parameters may be calculated as [1]

$$\left(\frac{\overline{S}}{d}\right)_{\mathrm{mix}} = \sum_i \left(\frac{\overline{S}}{d}\right)_i \tag{18}$$

and

$$\left[\left(\frac{b}{d}\right)_{\mathrm{mix}}\left(\frac{\overline{S}}{d}\right)_{\mathrm{mix}}\right]^{1/2} = \sum_i \left[\left(\frac{b}{d}\right)_i\left(\frac{\overline{S}}{d}\right)_i\right]^{1/2} \tag{19}$$

where the broadening parameter $(b/d)_i$ for each gas depends on the gas mole fraction as $(b/d)_i = (b/d)_{is}x_i + (b/d)_{ia}(1-x_i)$.

1.2.2. Correlated-k distributions

The $k(g)$ function obtained by numerically inverting the cumulative density distribution of absorption coefficient strengths, obtained from Malkmus parameters Eq. (13), may also be used to calculate the transmissivity of inhomogeneous paths. Assuming that the k-distribution functions are correlated [1], i.e., that the peaks and valleys of the absorption coefficient spectra are at roughly the same spectral locations, regardless of the state of the gas, the narrow-band transmissivity for inhomogeneous paths may be calculated as

$$\overline{\tau}(X) = \int_0^1 \exp\left(-\int_0^X k(X,g)\,\mathrm{d}X\right)\mathrm{d}g \tag{20}$$

where $k(X,g)$ is the cumulative distribution function evaluated from the local Malkmus parameters as above.

For inhomogeneous paths involving gas mixtures, the narrow-band mixing model of Modest and Riazzi [14] may be used to obtain the combined $g_{\mathrm{mix}}(k)$ function from the individual $g_i(k)$ functions for each gas i. For the special case of two gases, this equation reduces to

$$g_{\mathrm{mix}}(k_{\mathrm{mix}}) = \int_0^1 g_2(k_{\mathrm{mix}}-k_1)\,\mathrm{d}g_1 \tag{21}$$

2. Model development

This section details the development of a multiscale Malkmus model. It is proposed to divide the spectral lines within a narrow band into several uncorrelated groups based on their lower level energies of transition (E''), and to assign a characteristic value of E'' to each group. The Malkmus line intensity probability distribution function may then be modified to

$$p_j(S) = \frac{1}{\ln R}S^{-1}\left[\exp\left(-\frac{S}{S_{Mj}}\right)-\exp\left(-\frac{RS}{S_{Mj}}\right)\right] \quad j=1,2,\ldots,J \tag{22}$$

The mean value of S for the lines within a group j is then given by

$$\mathbf{S}_j = \int S p_j(S)\,\mathrm{d}S = \left[\frac{R-1}{R\ln R}\right]S_{Mj} \tag{23}$$

All the lines within a group j have line intensities, which scale up by the same factor $a_j(T)$ with temperature, where

$$a_j(T) \propto \exp\left(-\frac{hc}{k_bT}E_j''\right)T^{-n} \tag{24}$$

where h is Planck's constant, c is the speed of light, k_b is Boltzmann's constant and n is an exponent (assumed the same for all the groups), which accounts for the reduction in gas density at higher temperatures as well as the rotational partition function, and $a_j(T_0)=1$ at some reference temperature T_0. Thus, for each line within group j, the absorption coefficient at any given wavenumber is scaled up by a factor of $a_j(T)$. The intensities are known to vary linearly with partial pressure, i.e.,

$$S_j(T,P_j) = S_j(T_0,P_0)a_j(T)\frac{P_j}{P_0} \tag{25}$$

The equivalent width of a line at a temperature $T \neq T_0$ and total pressure $P \neq P_0$ for a homogeneous path follows as,

$$W_j = \int\left(1-\exp\left(-\kappa_j(\eta,T_0)a_j(T)X\right)\right)\mathrm{d}\eta \tag{26}$$

where X is the partial pressure path length. For a nonisothermal path, the equivalent width W_j is given by

$$W_j = \int\left[1-\exp\left(-\int_0^X \kappa\left(\eta,T(X'),P(X')\right)\mathrm{d}X'\right)\right]\mathrm{d}\eta \tag{27}$$

However, the temperature and total pressure dependence of the absorption coefficient are not only affected by the variation of the line intensity S [as given by Eq. (24)], but also by the temperature and total pressure dependencies of the line broadening in Eq. (5). These dependencies are inconvenient, and it is proposed to account for them by evaluating a path-averaged broadening parameter, as in the Curtis–Godson model. The exact form of this average will become clear later and, for the moment, the value of b in Eq. (5) is simply replaced by $\tilde{b}$, which is the path-averaged value. Thus,

$$W = \int\left[1-\exp\left(-\kappa(\eta,T_0)\int_0^X a_j\left(T(X')\right)\mathrm{d}X'\right)\right]\mathrm{d}\eta \tag{28}$$

For each group an equivalent pressure path may then be defined as

$$\sigma_j = \int_0^X a_j\big(T(X')\big)\,\mathrm{d}X' \tag{29}$$

Thus, the mean equivalent width for the lines belonging to the group j may be obtained by comparison with Eq. (6) as

$$W_j(S,\sigma_j) = S\sigma_j \exp\left(-\frac{S\sigma_j}{2\pi\tilde{b}_j}\right) \times \left[I_0\left(\frac{S\sigma_j}{2\pi\tilde{b}_j}\right) + I_1\left(\frac{S\sigma_j}{2\pi\tilde{b}_j}\right)\right] \tag{30}$$

Within group j, the probability distribution of line intensities is given by $p_j(S)$ in Eq. (22). Thus, the mean equivalent line width for group j is,

$$\overline{W}_j = \int W_j p_j(S)\,\mathrm{d}S = \frac{2\pi\tilde{b}}{\ln R}\left[\left(1+\frac{S_{Mj}\sigma_j}{\pi\tilde{b}_j}\right)^{1/2} - \left(1+\frac{S_{Mj}\sigma_j}{R\pi\tilde{b}_j}\right)^{1/2}\right] \tag{31}$$

The narrow-band transmissivity for group j follows then as

$$\overline{\tau_j} = \exp\left(-\frac{\overline{W_j}}{d}\right) = \exp\left(\left[-\frac{\pi\tilde{b}_j}{2d}\left\{\left(1+\frac{\overline{S}_j\sigma_j}{\pi\tilde{b}_j}\right)^{1/2} - 1\right\}\right]\right) \tag{32}$$

Assuming the groups to be uncorrelated from one another, the overall transmissivity $\overline{\tau}$ becomes the product of the transmissivities of each group, i.e.,

$$\overline{\tau} = \prod_j \overline{\tau}_j \tag{33}$$

The narrow-band transmissivity for an inhomogeneous path then follows from Eq. (33) as

$$\overline{\tau} = \exp\left(\sum_j\left[-\frac{\pi\tilde{b}_j}{2d}\left\{\left(1+\frac{4\overline{S}_j\sigma_j}{\tilde{b}_j}\right)^{1/2} - 1\right\}\right]\right) \tag{34}$$

where $\tilde{b}_j$ is the path-averaged value of b_j, i.e.,

$$\tilde{b}_j = \frac{1}{\tilde{t}}\int_0^X \frac{\overline{S}}{d} b_j\,\mathrm{d}X \tag{35}$$

with $b_j = b_{sj}x + b_{aj}(1-x)$. The path-averaged value $\tilde{t}$ may be obtained from Eq. (16), while $\overline{S}/d$ may be obtained from the path average of the line intensity S_j, as a function of T and P, as described by Eq. (25). The line widths are assumed to vary with temperature and total pressure as [15]

$$b_j(T,P) = b_j(T_0,P_0)\left(\frac{T}{T_0}\right)^{n_{bj}}\frac{P}{P_0} \tag{36}$$

where n_{bj} is a parameter (assumed different for each group j) which accounts for the temperature dependence of the line widths.

The parameters for this model may be obtained from narrow-band transmissivities, which may come either from experiment, or from line-by-line databases. Obviously, a choice needs to be made for the number of groups. At first glance it may seem that the model would perform progressively better with increasing number of groups, it should be noted that the assumption of uncorrelated groups may break down with larger number of scales. Thus, there may exist an optimum number of scales, which has to be found through trial and error. However, one may also suspect that increasing the number of groups beyond two or three will provide little increase in accuracy accompanied by substantial increase in calculation cost. Thus, in the current work, two groups were chosen to model narrow-band transmissivities obtained from line-by-line databases.

Experimental narrow-band transmission data at various temperatures may also be used to obtain the MSM parameters. In this case, the data for low temperatures may be initially used to obtain the parameters for the first group. The transmission data at higher temperatures are then divided by the transmissivities predicted by using only the first group. These divided transmissivities may then be used to obtain the parameters for the next group, and so on, until a sufficient number of groups have been obtained.

3. Model validation

The multi-scale model assumes the existence of several groups of lines within a narrow band, with a characteristic value of the base energy of transition (E'') for each group, with the overall transmissivity being the product of the transmissivities of each group. This assumption was validated by comparing the narrow-band transmissivities obtained from the HITEMP [16] and CDSD [17] high-resolution spectral databases for H_2O and CO_2, respectively, with the product of narrow-band transmissivities obtained by only considering lines in each database, whose base energies of transition lie within certain ranges, as follows.

The lines in the CDSD and HITEMP databases were separated into two groups, one of which consisted of lines whose base energy of transition (E'') was less than a certain cutoff value, E''_c, and the other consisting of lines with $E'' > E''_c$. For CO_2, E''_c was set at 3000 cm^{-1}, while for H_2O, a value of 1000 cm^{-1} was chosen for E''_c. These values were chosen so as to have a significant contribution to absorption at all the gas bands from both groups at 1000 K.

Line-by-line narrow-band transmissivities were calculated for various homogeneous paths, for two different cases for each gas. Spectral narrow-band transmissivities are calculated for each case using line data from the CDSD database for CO_2 and the HITEMP database for H_2O. The local absorption coefficients are evaluated at thirteen quadrature points along the path, and the benchmark line-by-line transmissivity is calculated using the equation

$$\overline{\tau}_{lbl} = \frac{1}{\Delta\eta}\int_{\Delta\eta}\exp\left(-\int_0^X \kappa_\eta\,\mathrm{d}X\right)\mathrm{d}\eta \tag{37}$$

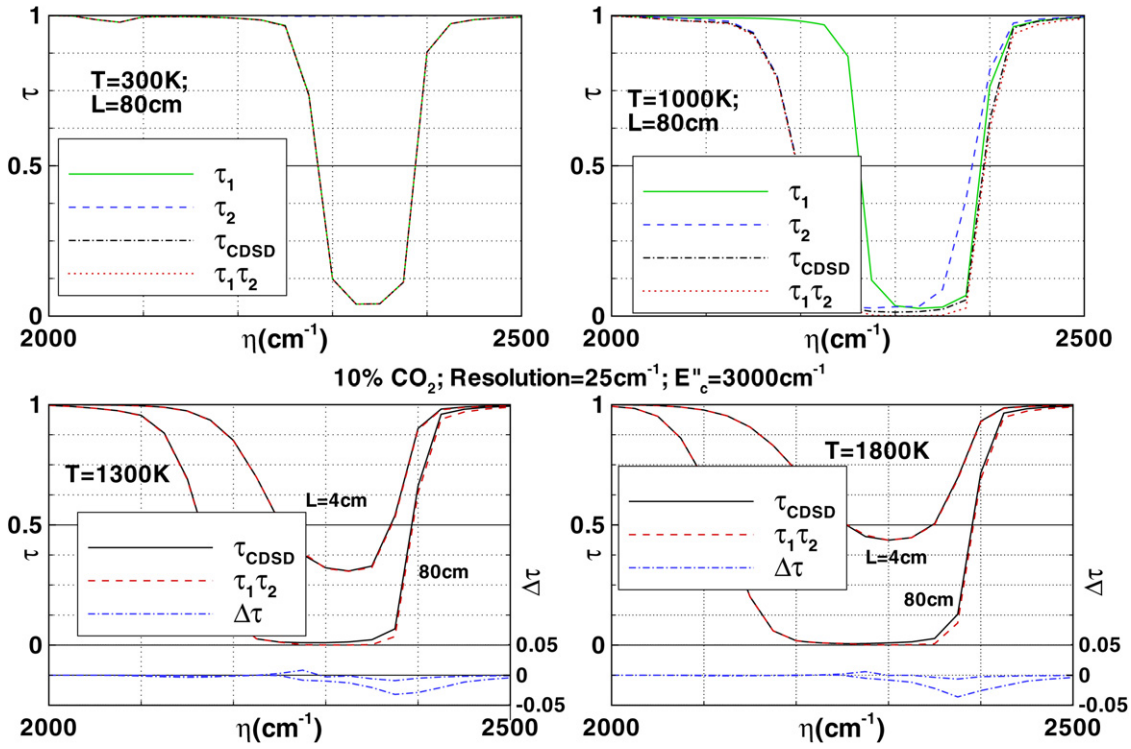

Fig. 1. Comparison of CDSD transmissivities with the transmissivities of each group (300 K to 1800 K at 25 cm^{-1} resolution).

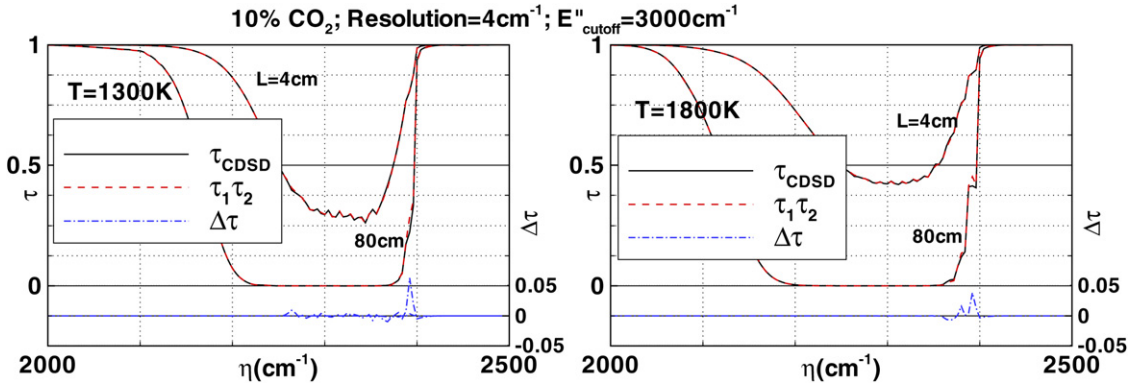

Fig. 2. Comparison of CDSD transmissivities with the product of transmissivities of two groups (1300 K, 1800 K at 4 cm^{-1} resolution).

where $\Delta\eta$ is the spectral resolution. The first case only considered lines from the low-temperature group for each gas, while the second case considered lines from the high-temperature group alone. The product of the 'low-temperature' and 'high-temperature' transmissivities was then compared with the transmissivity obtained by considering all the lines in the database. The plots shown in this section are representative plots, and further validation figures may be found in [18].

The top half of Fig. 1 shows the transmissivities for each group for the 4.3 μm band of CO_2 at 300 K and 1000 K at 25 cm^{-1} resolution, for a path length of 80 cm. Other lengths were also considered, namely, 10 cm, 20 cm, 40 cm and 50 cm. The low-temperature group dominates absorption at 300 K, with negligible contribution from the high-temperature group, as the figure shows. Thus, there is very little error between the product of the group transmissivities and the actual transmissivity at this temperature. At 1000 K, the high-temperature group contributes significantly to absorption at the band center, while essentially dominating absorption in the band wings, leading to 'broadening' of the band. The bottom half of Fig. 1 shows the product of the transmissivities of each group compared with the transmissivity obtained directly by considering all the lines in the CDSD database for a homogeneous gas path at 25 cm^{-1} resolution, also for the 4.3 μm band of CO_2 for path lengths of 4 and 80 cm and temperatures of 1300 K and 1800 K. As the figure shows, the products of the group transmissivities are very close to the actual line-by-line transmissivities calculated from the CDSD database, with a maximum absolute error in the narrow-band transmissivity (for all the path lengths considered) of about 0.03.

Fig. 2 shows a similar plot to that of the bottom half of Fig. 1, with a 4 cm^{-1} resolution. Similarly, Fig. 3 compares

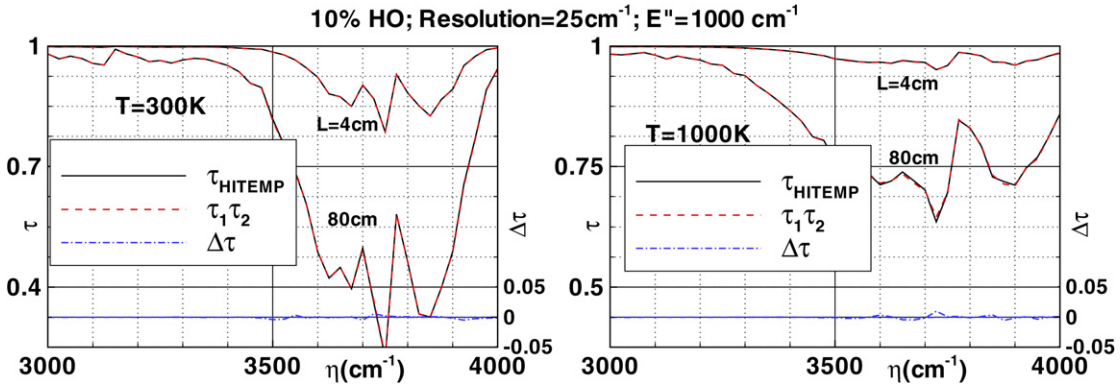

Fig. 3. Comparison of HITEMP transmissivities with the product of transmissivities of two groups (300 K, 1000 K at 25 cm^{-1} resolution for H_2O).

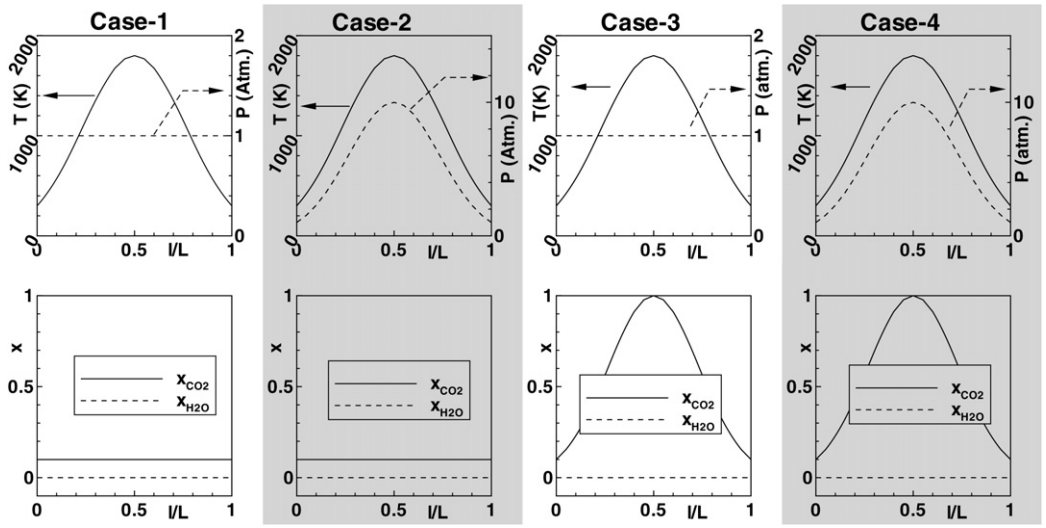

Fig. 4. Variation of temperature, total pressure and mole fraction along an inhomogeneous gas path: Cases 1 through 4 (CO_2 only).

the products of the transmissivities of each group with the composite transmissivities for the 2.7 μm water vapor band at 25 cm^{-1} resolution, with line data taken from HITEMP. Again, other path lengths were considered for these cases with similar results. From analysis of the data, it was seen that the low-temperature group dominates absorption at 300 K, with just a small contribution from the high-temperature group. At 1000 K, both groups contribute significantly to absorption at the band center. However, the contribution of the low-temperature group declines in the band wings at this temperature, due to the rotational partition function and the reduction of gas density at higher temperatures, with the high-temperature group contributing almost exclusively to absorption in these regions. The products of group transmissivities are again very close to the actual transmissivities, with the maximum error being less than 0.01. The products of the low-temperature and high-temperature transmissivities are also compared with the composite transmissivity for inhomogeneous paths. The path integral of the absorption coefficient was evaluated using a second order Newton–Cotes scheme, using the 13 quadrature points. The effect of using more quadrature points was also investigated, and 13 points were deemed sufficient for the cases at hand, with the error between using 27 points and 13 points being less than 1%. Fig. 4 shows the variation of T, P and x_{CO_2} for various inhomogeneous paths for CO_2/N_2 mixtures. Case 1 considers a Gaussian temperature field, with $T = 1800$ K at the center of the path and $T = 300$ K at the edges, with the pressure and mole fraction of CO_2 being constant throughout the path. Case 2 has a Gaussian variation of both temperature and total pressure, while case 3 has constant total pressure and Gaussian temperature and mole fraction fields. Case 4 considers a Gaussian variation of all three parameters. The products of the group transmissivities (at 4 cm^{-1} resolution) for cases 1 and 2 are compared with the line-by-line transmissivity for the 2.7 μm band obtained from the CDSD database in the left half of Fig. 5. It is seen from the figure that the maximum error in the narrow-band transmissivity does not exceed 0.01 for any of the cases shown. The error is highest at the center of the band, and negligible in the band wings. This is understandable, because the high-temperature group is expected to dominate absorption in the band wings, as seen from the top half of Fig. 1. The high-temperature group is most dominant in the band wings for case 2, because the total pressure is highest at the centerline, where the temperature is also highest, as seen from the second panel of Fig. 4.

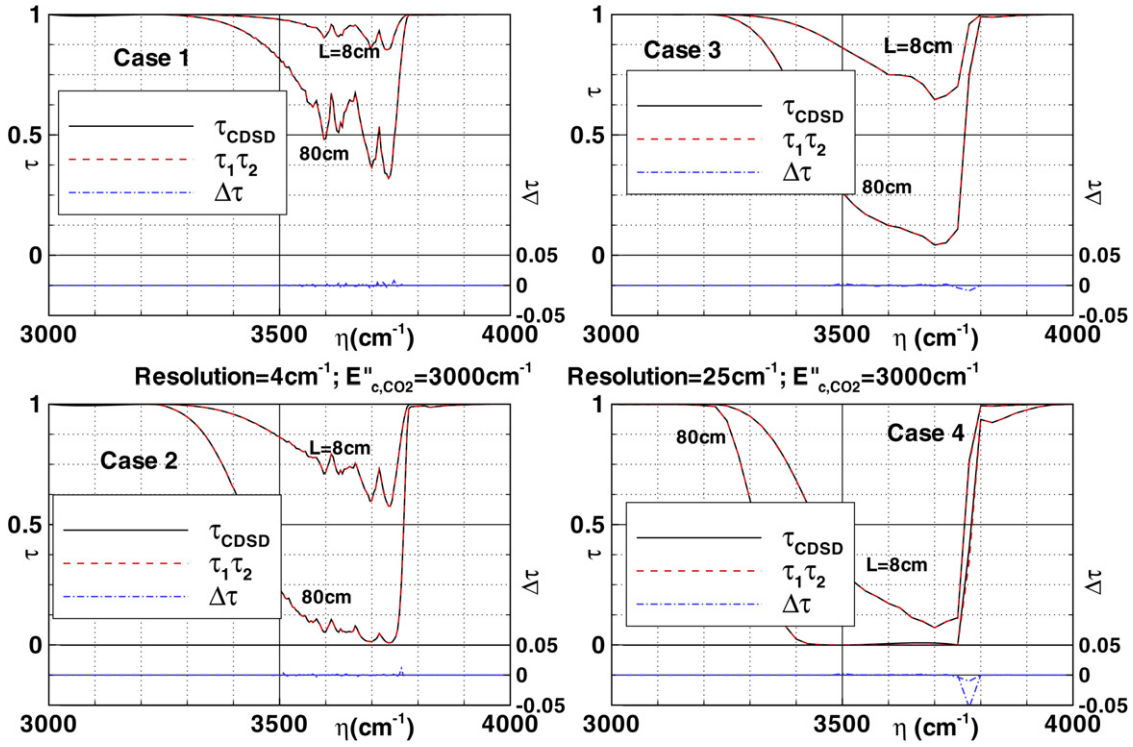

Fig. 5. Comparison of CDSD transmissivities with the product of transmissivities of two groups (CO_2, 2.7 μm band).

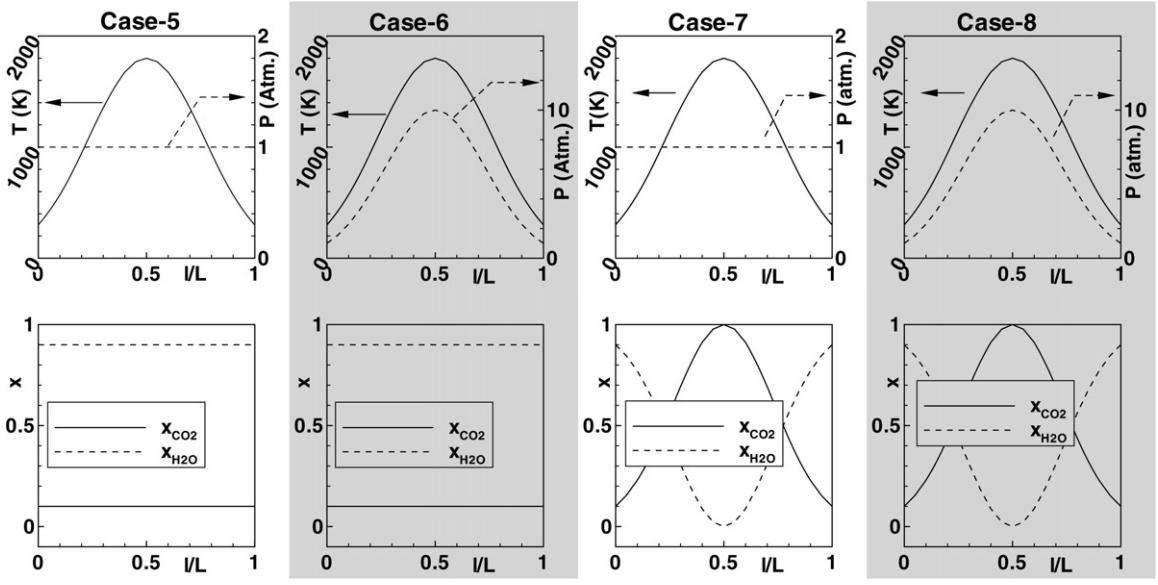

Fig. 6. Variation of temperature, total pressure and mole fraction along an inhomogeneous gas path: Cases 5 through 8.

The right half of Fig. 5 compares the same transmissivities for cases 3 and 4 for a 25 cm^{-1} resolution. It can be seen from the figure that the error is negligible over most of the band, with an average band error of less than 0.01. The line-by-line transmissivity may thus be accurately modeled as the product of transmissivities of two groups.

The product of the group transmissivities was also compared with the composite transmissivity for inhomogeneous paths consisting of mixtures of CO_2 and H_2O for the 2.7 μm spectral region where both gases have important, overlapping bands. Fig. 6 shows the variation of T, P, x_{CO_2} and x_{H_2O} along the paths considered, while Fig. 7 compares the product of the low-temperature and high-temperature transmissivities with the transmissivity obtained by considering all the lines in the CDSD database for CO_2, and the HITEMP database for H_2O. As the figure shows, the pure error in transmissivity is more evenly distributed over the band than for the CO_2 cases. This is because the mole fractions of CO_2 and H_2O are counter-varying, which means the high-temperature group of CO_2 and the low-temperature group of H_2O contribute most to absorp-

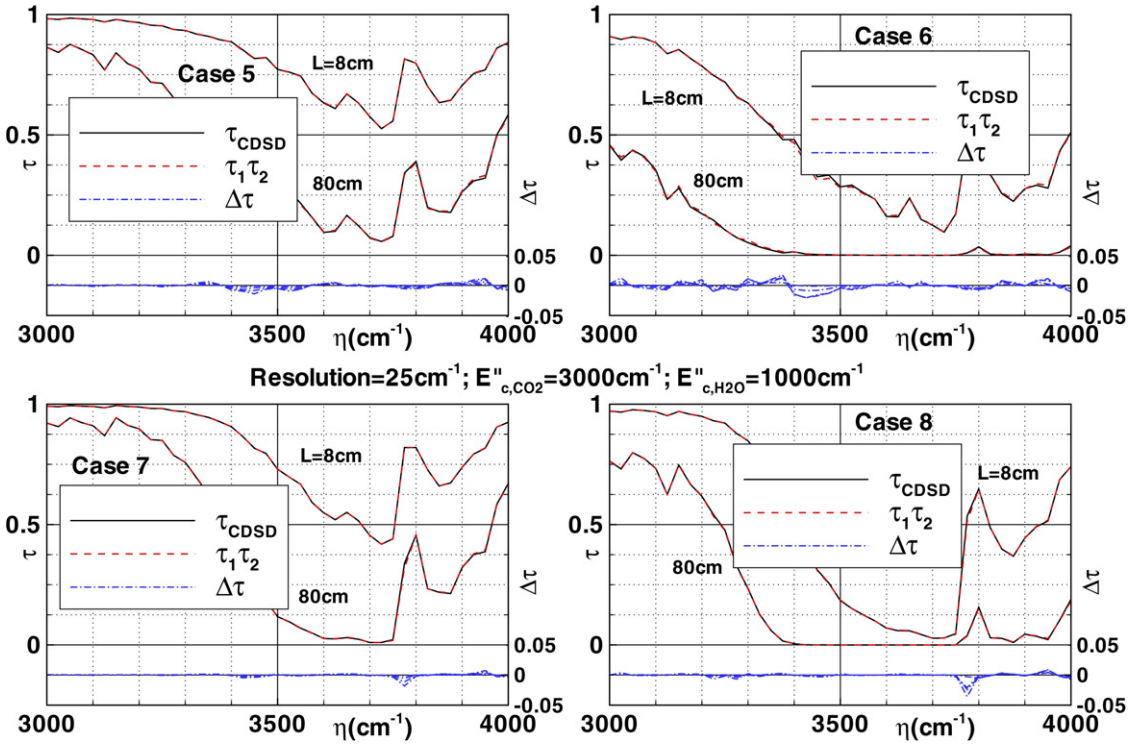

Fig. 7. Comparison of CDSD transmissivities with the product of transmissivities of two groups (Cases 5 to 8, 25 cm^{-1} resolution).

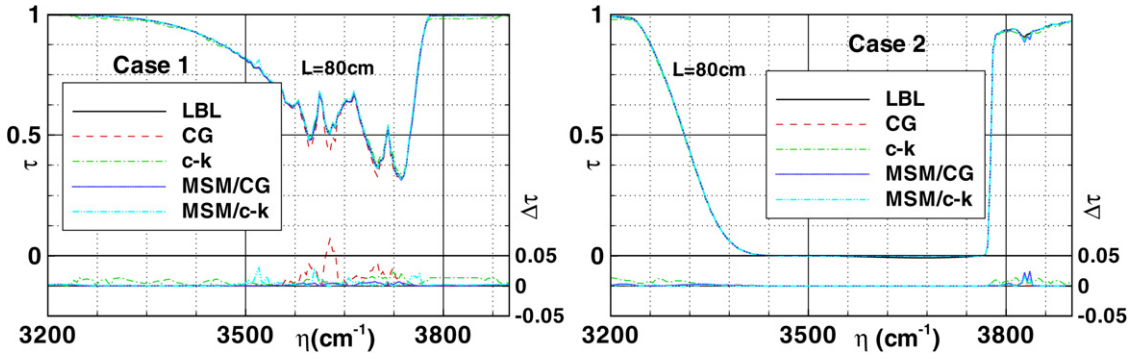

Fig. 8. Comparison of line-by-line, CG, c–k and MS models for cases 1 and 2, 4 cm^{-1} resolution.

tion in the band wings, and vice-versa in the center of the band. The average error for cases 5 and 6 are of the order of 0.02, with a maximum error of about 0.05, while for cases 7 and 8 the average errors are around 0.01, with maximum errors of 0.025.

It is seen from the above figures that the narrow-band transmissivity may be approximated as the product of the transmissivities of two groups with little error.

4. Results and discussion

The multi-scale Malkmus model is compared to the Curtis–Godson and correlated-k approaches for various test cases. The same cases as previously presented in Figs. 4 and 6 are considered again. Local Malkmus parameters were also calculated at each quadrature point by least-squares fitting transmissivity data obtained from the CDSD and HITEMP database, for homogeneous paths at the local state (T, P, x). These parameters are used to obtain the Curtis–Godson transmissivities for the inhomogeneous path from Eqs. (15)–(17). The local Malkmus parameters were also used to obtain local k-distributions, which were plugged into Eq. (20) to obtain transmissivities for the inhomogeneous paths using the correlated-k method. The integral in Eq. (20) was evaluated using the same quadrature scheme as for the Curtis–Godson method.

Finally, transmission data for homogeneous paths at the local states are used to obtain the multi-scale Malkmus parameters as outlined above. These parameters are then employed to obtain an estimate for the transmissivity of the inhomogeneous path using both the Curtis–Godson and correlated-k methods. The following sections present sample plots comparing the MSM/CG and MSM/c–k models with the (single scale) CG and c–k methods. More extensive comparisons may be found in [18].

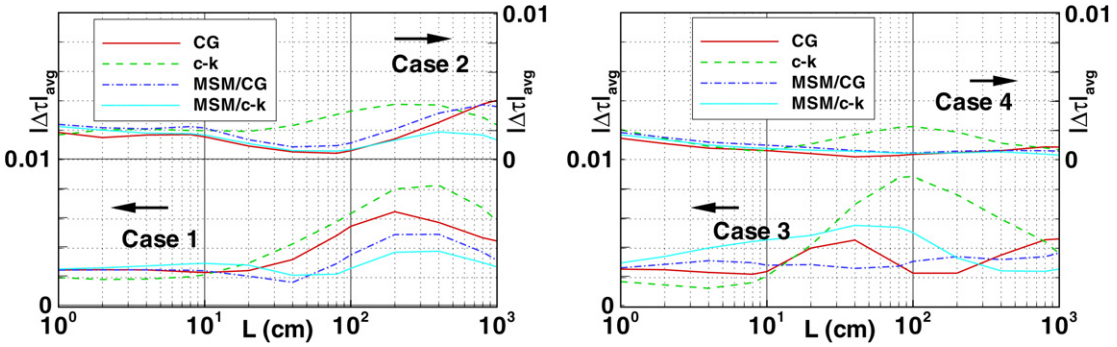

Fig. 9. Comparison of line-by-line, CG, c–k and MS models (4 cm^{-1} resolution, band-averaged absolute error in τ for all cases for the 2.7 μm band of CO_2).

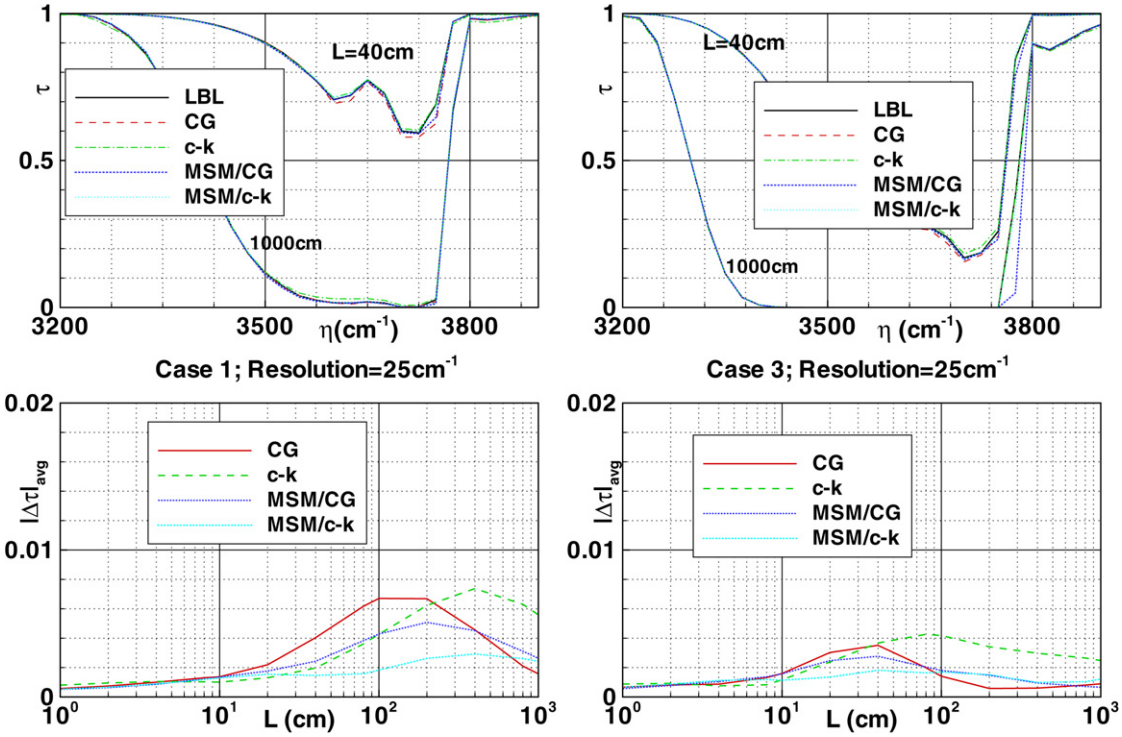

Fig. 10. Comparison of line-by-line, CG, c–k and MS models for cases 1 and 3, 25 cm^{-1} resolution, 2.7 μm band of CO_2.

4.1. Carbon dioxide

The MSM/CG and MSM/c–k models are first compared to the single scale CG approximation and the c–k method for the test cases of Fig. 4, i.e., for CO_2/N_2 mixtures with variations in T, P and x_{CO_2} as shown.

Fig. 8 compares the Curtis–Godson, correlated-k, MSM/CG and MSM/c–k transmissivities for cases 1 and 2 with the benchmark LBL transmissivities at 4 cm^{-1} resolution. All methods provide reasonable estimates of the narrow-band transmissivity for case 2. However, for case 1, the Curtis–Godson approximation is seen to overestimate absorption at the center of the band. The correlated-k method does better in this region, while overestimating absorption near the wings. The MSM/CG and MSM/c–k methods both provide even better estimates of the narrow-band transmissivity.

Fig. 9 shows the wide-band averaged absolute error in the narrow-band transmissivity for the 2.7 μm band of CO_2 for all four cases. The MS models perform better than CG and c–k for cases 1 and 3, while all four methods are comparable for cases 2 and 4.

The left half of Fig. 10 compares the MSM models with the Curtis–Godson and correlated-k models for case 1 for the 2.7 μm band of CO_2 at 25 cm^{-1} resolution. The bottom half of the figure shows the average absolute error in narrow-band transmissivity, which is obtained by adding the absolute errors over the band and dividing by the number of data points. As the figure shows, all models do well for the optically thin cases for the 2.7 μm band of CO_2, with the CG and c–k methods doing significantly worse than the MS methods for optically intermediate cases.

The CG, c–k, MSM/CG and MSM/c–k methods are compared with the benchmark line-by-line transmissivities for case 3 in the right half of Fig. 10. The c–k method is seen to perform the worst, with the CG, MSM/CG and MSM/c–k methods yielding comparable errors.

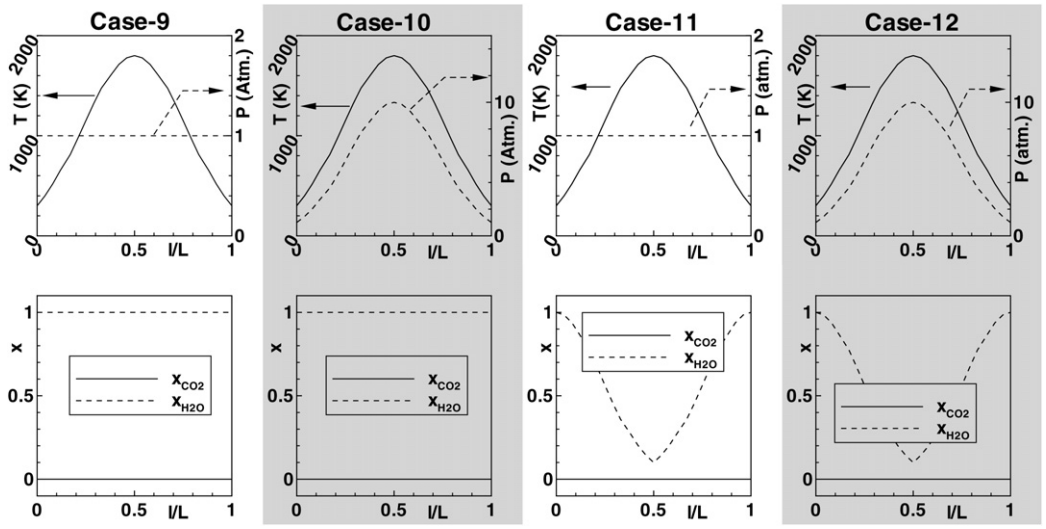

Fig. 11. Variation of temperature, total pressure and mole fraction along an inhomogeneous gas path: Cases 9 through 12 (for H_2O).

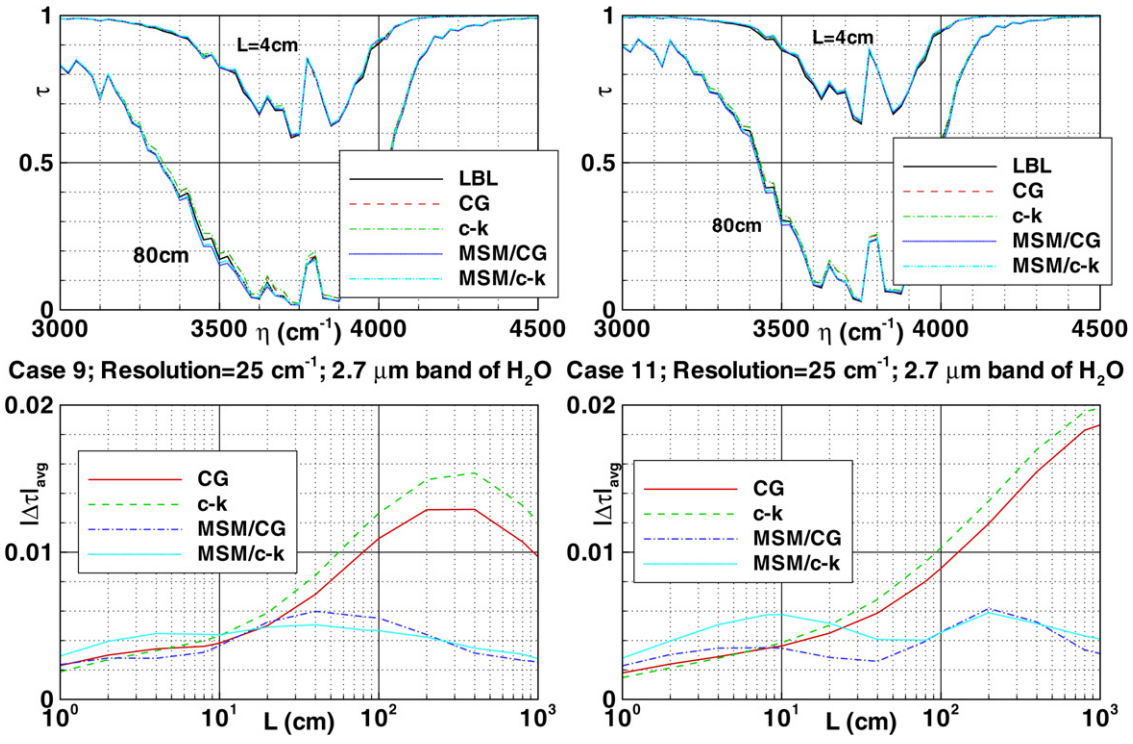

Fig. 12. Comparison of line-by-line, CG, *c–k* and MS models for the 2.7 μm band of H_2O at 25 cm^{-1} resolution: Cases 9 and 11.

4.2. Water vapor

The MSM/CG and MSM/*c–k* models were also compared to the CG approximation and the *c–k* model for the 6.3, 2.7 and 1.8 μm bands of H_2O. Fig. 11 shows the variation of T, P and x along the inhomogeneous gas paths considered for H_2O. Case 9 involves a Gaussian variation of temperature along the path, with $T = 300$ K at the edges and $T = 1800$ K at the center. The total pressure and H_2O mole fraction are constant along the path. Case 10 incorporates (in addition to the exponential temperature field of case 9) a Gaussian variation of the total pressure, from $P = 10$ bar at the centerline to $P = 1$ bar at the edges of the path. Case 11 considers variations in temperature and H_2O mole fraction, while case 12 involves Gaussian T, P and x_{H_2O} fields as shown in the right half of the same figure.

The left half of Fig. 12 compares the MSM models with the Curtis–Godson and correlated-*k* models for case 9 for the 2.7 μm band of H_2O at 25 cm^{-1} resolution. The CG and *c–k* models yield much larger errors relative to the MS models, as seen in the figure.

The MSM/CG and MSM/*c–k* methods do significantly better than the CG approximation and the *c–k* method for case 11, as the right half of Fig. 12 shows. The average absolute error in

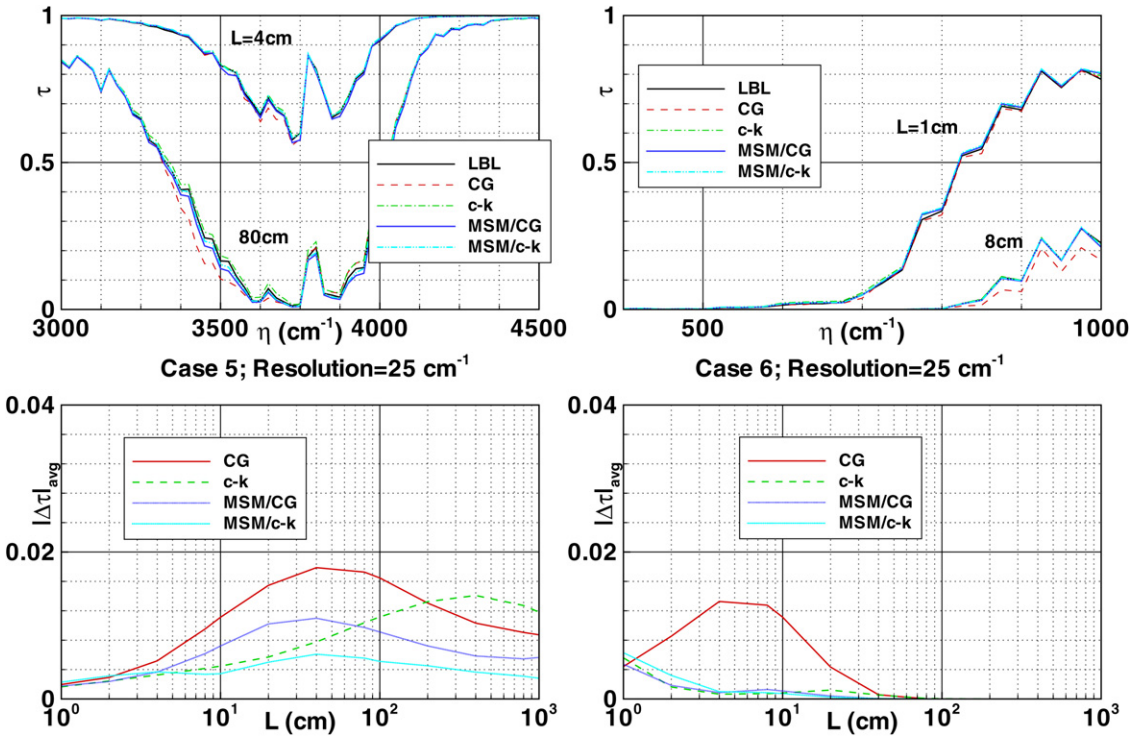

Fig. 13. Comparison of line-by-line, CG, c–k and MS models at 25 cm^{-1} resolution: Case 5, 3000 to 4500 cm^{-1}; and case 6, 400 to 1000 cm^{-1}.

the narrow-band transmissivity for the MS methods is roughly a third that of the CG and c–k cases, as the figure shows.

4.3. CO_2/H_2O mixtures

For the case of CO_2/H_2O mixtures, two spectral regions are chosen for comparison between the methods, viz., 400 to 1000 cm^{-1} and 3000 to 4500 cm^{-1} i.e., the regions where the overlap between the gas bands of CO_2 and those of H_2O are the strongest. The 400 to 1000 cm^{-1} region involves interactions between the 15 μm band of CO_2 and the rotational band of H_2O, while the 3000 to 4500 cm^{-1} region shows overlap between the 2.7 μm bands of both gases.

The left half of Fig. 13 compares the MSM/CG and MSM/c–k models with the Curtis–Godson and correlated-k models for the inhomogeneous path of case 5, depicted in the first panel of Fig. 6 at 25 cm^{-1} resolution. The MSM/CG model performs better than the CG approximation (which is seen to significantly overpredict absorption) for all the lengths considered in the 3000 to 4500 cm^{-1} region, and better than the c–k model for the optically thick paths. The MSM/c–k model is seen to yield the lowest error of all four models for this spectral region.

The right half of Fig. 13 compares the MSM models with the Curtis–Godson and correlated-k models for the inhomogeneous path of case 6, shown in the second panel of Fig. 6, for the 400–1000 cm^{-1} spectral region. The CG approximation again shows lower transmission than the line-by-line case, yielding errors nearly five times as large as those of the other methods. The other methods yield comparable errors, with the MS models performing somewhat better than c–k for the optically thin cases. The c–k method performs somewhat better than the MS models for the optically thin paths, with all four methods yielding low errors for the optically intermediate/optically thick paths.

5. Conclusions

A multi-scale Malkmus model has been developed to predict accurate transmissivities for inhomogeneous gas paths. The model was compared to the current state-of-the-art approaches, viz., the Curtis–Godson and the correlated-k approaches. For gas paths containing CO_2/N_2 mixtures, the CG and c–k models generally perform well, and the MS models further improve accuracy. For mixtures, including water vapor, the MSM/CG and MSM/c–k approaches are substantially more accurate than the CG approximation and the c–k model. For severely inhomogeneous gas paths with water-vapor or CO_2/H_2O mixtures, the MS models yield maximum errors, which are between a half to a fifth of those of the CG and c–k approximations. The CG model is seen to significantly overpredict absorption in certain spectral regions for CO_2/H_2O mixtures, while the c–k model is often seen to underpredict absorption for the same cases. The MS models perform especially well as compared to CG and c–k for optically intermediate cases, where the traditional methods show the largest errors.

Acknowledgement

Funding from the National Science Foundation (Grant number CTS-0112423) is gratefully acknowledged.

References

[1] M.F. Modest, Radiative Heat Transfer, second ed., Academic Press, New York, 2003.

[2] R.M. Goody, Y.L. Yung, Atmospheric Radiation – Theoretical Basis, second ed., Oxford University Press, New York, 1989.

[3] H.C. Hottel, A.F. Sarofim, Radiative Transfer, McGraw-Hill, New York, 1967.

[4] W.M. Elsasser, Heat Transfer by Infrared Radiation in the Atmosphere, Harvard University Press, Cambridge, MA, 1943.

[5] J.-M. Hartmann, R. Levi Di Leon, J. Taine, Line-by-line and narrow-band statistical model calculations for H_2O, Journal of Quantitative Spectroscopy and Radiative Transfer 32 (2) (1984) 119–127.

[6] W.L. Godson, The computation of infrared transmission by atmospheric water vapour: I and II, Journal of Meteorology 12 (1955) 272 and 533.

[7] R.M. Goody, A statistical model for water-vapour absorption, Quarterly Journal of the Royal Meteorological Society 78 (1952) 165.

[8] R.M. Goody, Atmospheric Radiation, Oxford University Press, Oxford, 1964.

[9] C.B. Ludwig, W. Malkmus, J.E. Reardon, J.A.L. Thomson, Handbook of infrared radiation from combustion gases, Technical Report SP-3080, NASA, 1973.

[10] G.N. Plass, Models for spectral band absorption, Journal of the Optical Society of America 48 (10) (1958) 690–703.

[11] W. Malkmus, Random Lorentz band model with exponential-tailed S^{-1} line-intensity distribution function, Journal of the Optical Society of America 57 (3) (1967) 323–329.

[12] S.J. Young, Nonisothermal band model theory, Journal of Quantitative Spectroscopy and Radiative Transfer 18 (1977) 1–28.

[13] A.A. Lacis, V. Oinas, A description of the correlated-k distribution method for modeling nongray gaseous absorption, thermal emission, and multiple scattering in vertically inhomogeneous atmospheres, Journal of Geophysical Research 96 (D5) (1991) 9027–9063.

[14] M.F. Modest, R.J. Riazzi, Assembly of full-spectrum k-distributions from a narrow-band database effects of mixing gases, gases and nongray absorbing particles, and mixtures with nongray scatterers in nongray enclosures, Journal of Quantitative Spectroscopy and Radiative Transfer 90 (2) (2004) 169–189.

[15] L.S. Rothman, R.B. Wattson, R.R. Gamache, J. Schroeder, A. McCann, HITRAN, HAWKS and HITEMP high temperature database, Proceedings of SPIE 2471 (1995) 105–111.

[16] L.S. Rothman, C. Camy-Peyret, J.-M. Flaud, R.R. Gamache, A. Goldman, D. Goorvitch, R.L. Hawkins, J. Schroeder, J.E.A. Selby, R.B. Wattson, HITEMP, the high-temperature molecular spectroscopic database. Available through: http://www.hitran.com.

[17] S.A. Tashkun, V.I. Perevalov, J.-L. Teffo, A.D. Bykov, N.N. Lavrentieva, CDSD-1000, the high-temperature carbon dioxide spectroscopic databank, Journal of Quantitative Spectroscopy and Radiative Transfer 82 (1–4) (2003) 165–196. Available from: ftp://ftp.iao.ru/pub/CDSD-1000.

[18] S.P. Bharadwaj, Medium resolution transmission measurements of CO_2 and H_2O at high temperature and a multiscale Malkmus model for treatment of inhomogeneous gas paths, PhD thesis, The Pennsylvania State University, Department of Mechanical Engineering, University Park, PA, 2005.